Journal of Environmental Chemical Engineering 9 (2021) 105863

Contents lists available at ScienceDirect

Journal of Environmental Chemical Engineering

journal homepage: www.elsevier.com/locate/jece

Modeling of sorption enhanced steam methane reforming in an adiabatic packed bed reactor using various CO_2 sorbents

M. Mateen Shahid [a], Syed Zaheer Abbas [a,b,*], Fahad Maqbool [a,c], Sergio Ramirez-Solis [d], Valerie Dupont [d], Tariq Mahmud [d]

[a] Chemical Engineering Department, University of Engineering and Technology Lahore, Pakistan
[b] Department of Chemical Engineering & Analytical Science, The University of Manchester, Manchester M13 9PL, United Kingdom
[c] Department of Chemical Engineering, Sharif College of Engineering and Technology, Lahore, Pakistan
[d] School of Chemical and Process Engineering (SCAPE), University of Leeds, Leeds LS2 9JT, United Kingdom

ARTICLE INFO

Editor: Teik Thye Lim

Keywords:
Sorption-enhanced steam methane reforming
Sorbent
CO_2 capture
Modeling
CH_4 conversion enhancement

ABSTRACT

A 1-D heterogeneous model of sorption-enhanced steam methane reforming (SE-SMR) process in a packed bed reactor consisting of nickel catalyst well mixed with CO_2 sorbent particles is investigated for three types of common sorbents. The performance of SE-SMR process is studied under low medium pressure conditions (3 – 11 bar) to find the optimum operating conditions. Optimal CaO sorption corresponding to 82% CH_4 conversion and 85% H_2 purity is found at 900 K, 3 bar, 3.5 $kgm^{-2}s^{-1}$ and S/C of 3.0. In contrast, lithium zirconate (LZC) and hydrotalcite (HTC) sorbents exhibited best sorptions under the operating conditions of 773 K, 5 bar and S/C of 3 with CH_4 conversion of 91.3% and 55.2%, and H_2 purity of 94.1% and 77.8% respectively. In these conditions, the CH_4 conversion increased by 114%, 111% and 67% compared to the conventional SMR for the processes enhanced by HTC, LZC and CaO sorption respectively.

1. Introduction

The SMR process is the most widely used technology for the commercial production of H_2 [1,2]. The conventional SMR process is usually carried out under high temperature (1073 – 1273 K) and pressure (20 – 35 bar) conditions in the presence of reforming catalyst (mostly Ni-based) [3].

$$CH_{4(g)} + H_2O_{(g)} \leftrightarrow CO_{(g)} + 3H_{2(g)} \qquad \Delta H^0_{298K} = 206.2 kJ mol^{-1}_{CH_4} \qquad (R1)$$

$$CH_{4(g)} + 2H_2O_{(g)} \leftrightarrow CO_{2(g)} + 4H_{2(g)} \qquad \Delta H^0_{298K} = 165 kJ\ mol^{-1}_{CH_4} \qquad (R2)$$

The excess steam from R1 then reacts with CO in a water gas shift (WGS) reactor by the WGS reaction (R3) to further maximize the H_2 yield [4].

$$CO_{(g)} + H_2O_{(g)} \leftrightarrow CO_{2(g)} + H_{2(g)} \qquad \Delta H^0_{298K} = -41.2 kJ\ mol^{-1}_{CO} \qquad (R3)$$

The reforming and WGS are limited by chemical equilibrium and the thermodynamic constraints preclude both reactions to attain complete conversions of CH_4 and CO in a single reactor [3,5]. Further, one ton of H_2 produced through SMR process releases approximately 8 ton of CO_2 into the atmosphere [6]. This excessive release of CO_2 gives a low H_2 selectivity and low H_2 yield [7]. These drawbacks of the SMR process stimulated the researchers to develop more environment friendly and less energy intensive processes for the production of H_2. One such innovative technology uses sorbents during the reforming reaction for uptake of CO_2 in-situ while producing H_2 enriched gas (up to 97% dry basis) in a single reactor [8]. This concept is termed as sorption-enhanced steam methane reforming (SE-SMR). In the SE-SMR process, reforming reactions (R1 & R2), WGS (R3) and sorption reaction (R4) takes place at the same time in a single packed bed reactor [9]. According to Le Chatelier's principle, the CO_2 removal would shift the overall reforming process towards more H_2 production [8]. The CO_2 sorption reaction is given as;

$$CO_{2(g)} + \varepsilon_{(s)} \rightarrow CO_2\varepsilon_{(s)} \qquad (R4)$$

Where, $\varepsilon_{(s)}$ is the CO_2 sorbent which may truly react with CO_2 to form a solid carbonate or may be physically or chemically adsorbed on the surface of the sorbent [2]. The overall SE-SMR reaction would become;

$$CH_{4(g)} + 2H_2O_{(g)} + \varepsilon_{(s)} \leftrightarrow CO_2\varepsilon_{(s)} + 4H_{2(g)} \qquad (R5)$$

The sorption of CO_2 is an exothermic process in which the

* Corresponding author at: Chemical Engineering Department, University of Engineering and Technology Lahore, Pakistan.
E-mail address: syedzaheer.abbas@manchester.ac.uk (S.Z. Abbas).

https://doi.org/10.1016/j.jece.2021.105863
Received 18 February 2021; Received in revised form 6 May 2021; Accepted 11 June 2021
Available online 15 June 2021

Nomenclature

a_v	Interfacial area per unit volume, m^2m^{-3}
b_{CO2}	Temperature dependent Langmuir parameter, kPa^{-1}
$b_{CO2,\ ref}$	Temperature dependent Langmuir parameter at reference conditions, kPa^{-1}
C_i	Concentration of component i, mol m^{-3}
$C_{i,in}$	Concentration of component i at inlet, mol m^{-3}
$C_{i,o}$	Concentration of component i at t = 0, mol m^{-3}
$C_{i,s}$	Concentration of component i on solid surface, mol m^{-3}
C_{pg}	Heat capacity of gas, J $kg^{-1}K^{-1}$
$C_{p,bed}$	Heat capacity of bed, J $kg^{-1}K^{-1}$
D_i	Effective diffusion coefficient, $m^2\ s^{-1}$
D_m	Average molecular diffusivity, $m^2\ s^{-1}$
d_P	Particle diameter of catalyst, m
D_p	Pore diffusion coefficient, $m^2\ s^{-1}$
D_z	Axial dispersion coefficient, $m^2\ s^{-1}$
E_j	Activation energy of reaction j, J mol^{-1}
E_{ad}	Activation energy of sorbents, J mol^{-1}
C_F	Conversion enhancement factor (%)
G_s	Gas mass flow velocity, kg $m^{-2}\ s^{-1}$
h_f	Heat transfer coefficient, W $m^{-2}\ s^{-1}$
$J_{D,i}$	Chilton-Colburn j-factor for mass transfer
J_H	Chilton-Colburn j-factor for heat transfer
k	Thermal conductivity, W $m^{-1}\ K^{-1}$
k_{eff}	Effective thermal conductivity, W $m^{-1}\ K^{-1}$
$k_{g,i}$	Gas to solid mass transfer coefficient of component i, $m^3\ m^{-2}s^{-1}$
K_i	Sorption constant of species i
k_j	Kinetic constant of reaction j
$K_{o,i}$	Reference sorption constant of species i
K_j	Equilibrium constant of reaction j
k_z	Axial thermal conductivity, W $m^{-1}\ K^{-1}$
L	Length of reactor bed, m
m_{CO2}	Maximum sorption capacity for HTC, mol kg^{-1}
p_i	Partial pressure of specie i, bar
P	Total pressure, bar
p_i^{feed}	Partial pressure of component i in feed, bar
P°	Pressure at z = 0, bar
P_{in}	Inlet pressure of the feed, bar
P_r	Prandtl number
q_{CO2}	concentration of CO_2 on sorbent, mol kg^{-1}
$q_{CO2,\ max}$	Maximum carbonation conversion, mol kg^{-1}
R, R_g	Ideal gas constant, J $mol^{-1}K^{-1}$
r_i	Rate of formation of component i, mol $kg_{cat}^{-1}s^{-1}$
r_{ads}	Rate of sorption of CO_2, mol $kg^{-1}s^{-1}$
R_e	Reynolds number
R_j	Rate of reaction j, mol $kg_{cat}^{-1}s^{-1}$
S_{ci}	Schmidt's number
T	Temperature within reactor, K
T_{in}	Inlet temperature, K
T_s	Temperature of catalyst particles, K
$T_{s,o}$	Temperature of solid particles at 't = 0', K
u_s, v	Superficial velocity, m s^{-1}
X_{max}	Maximum fractional carbonation conversion of CaO
X_{CH4}	Fractional conversion of CH_4
X	Extent of reaction
ΔH_{rex}	Heat of reaction at standard conditions, J mol^{-1}
ΔH_{ads}	Heat of sorption reaction at standard conditions, J mol^{-1}
ΔP	Pressure drop across the bed reactor, bar

Greek Letters

Ω	Denominator term in the reaction kinetics
λ_z^f	Effective thermal conductivity, W $m^{-1}\ K^{-1}$
λ_g	Average gas thermal conductivity, W $m^{-1}\ K^{-1}$
λ_s	Solid thermal conductivity, W $m^{-1}\ K^{-1}$
λ_z°	Effective thermal conductivity of motionless fluid, W $m^{-1}\ K^{-1}$
ρ_f	Density of fluid, kg m^{-3}
ρ_{cat}	Density of catalyst, kg m^{-3}
ρ_{ad}	Density of sorbent, kg m^{-3}
η_j	Effectiveness factor
Φ_{ij}	Stoichiometric coefficient
μ_g	Viscosity of gas, Pa.s
υ	Ratio of amount of catalyst to amount of sorbent

equilibrium constant decreases with increase in temperature. The inclusion of exothermic carbonation reaction forms the overall SE-SMR process essentially thermo-neutral and little or no extra energy would be required during the SE-SMR process [10]. Moreover, the use of sorbents allows operating at comparatively lower temperatures (~873 K) than the conventional SMR process (950 – 1200 K) [11,12].

A considerable number of studies have been conducted on experimentation and modeling of the SE-SMR process so far [3,11,13]. Various sorbents such as zeolites, activated carbon, metallic oxides, dolomite, hematite and hydrotalcites (HTC) have been proposed for capturing CO_2 during SMR. SE-SMR operates at a relatively high temperatures (~873 K), which urges to study selective sorbents with suitable thermodynamics that retain significant uptake capacities in these conditions after repeated cycles of sorption-desorption, as well as fast kinetics [14,15]. Further, the sorbent must be easily regenerated and available at low cost [16]. Metal oxides such as CaO and lithium oxides show good capacities and kinetics at high temperatures (> 723 K). In regards with HTC, these sorbents can operate at medium-high temperatures without considerable effect on sorption kinetics but the CO_2 absorption capacity is modest as compared to other CO_2 sorbents [17].

In the last years, a wide number of investigations concerning to the SE-SMR process using CaO as a CO_2 sorbent have been carried out [2,13], [18,19], [20]. Unfortunately, the stability of CaO upon multiple carbonation – decarbonation cycles is the main concern [2,4]. To address this issue, researchers have tried to support CaO with inert compounds such Al_2O_3, MgO and $Ca_{12}Al_{14}O_{33}$ [21]. Lithium zirconate (LZC) finds advantages over CaO in terms of low regeneration temperature [22] Halabi et al. [23] investigated K-promoted HTC and LZC as potential sorbents in autothermal reforming. Several K-promoted HTC have been tested and equilibrium CO_2 sorption capacity of 0.40 $mol_{CO2}/kg_{\ sorbent}$ over 6000 cycles have been found [4]. High sorption capacity (2.09 $mol_{CO2}/kg_{\ sorbent}$) of HTC doped with potassium (20 wt%) was also measured by Joel et al. [5] at 3.1 bar.

However, no work has been conducted on the mathematical modeling of the SE-SMR process utilizing both a 18 wt% NiO-based catalyst and sorbents available in the literature. Also, no research evincing the optimal operating conditions like temperature, gas mass flux G_s, and S/C at low pressures (3–11 bar) for different sorbents (CaO, LZC and HTC) using SE-SMR process has been found. To fill this gap, a one-dimensional heterogeneous model of the SE-SMR process is developed and implemented in gPROMS for the solution of conservation equations. In this work, CaO, LZC, and HTC sorbents are used. The overall performance of the process is studied under the various operating conditions of temperature, pressure, S/C and gas mass flow velocity (G_s). The developed model is validated against the equilibrium data developed on an individual equilibrium software (chemical equilibrium with applications – CEA) and with the use of results estimated by Ding et al. [24] and Ochoa-Fernández et al. [25].

2. Mathematical modeling

2.1. State of the art SE-SMR kinetics of selected sorbents

In the modeling of the SE-SMR reactor, the rate equations and kinetics data for the SMR process is taken from Xu et al. [26] as shown in **Appendix A-1**. As in the SE-SMR process, the sorbent is added for removing the CO_2 produced during the reforming process. The reactions existent between CO_2 and CaO and overall SE-SMR are given as;

$$CaO_{(s)} + CO_{2(g)} \rightarrow CaCO_{3(s)} \qquad \Delta H^0_{298K} = -178.8 kJmol^{-1}_{CaO} \tag{R6}$$

$$CH_{4(g)} + 2H_2O_{(g)} + CaO_{(s)} \leftrightarrow CaCO_{3(s)} + 4H_{2(g)} \qquad \Delta H^0_{298K} = -13.9 kJmol^{-1}_{CaO} \tag{R7}$$

Many expressions have been published in the literature to explain the CO_2 capture kinetics of CaO [3,11,19]. The selection of kinetic models greatly depends upon the experimental procedures and morphology of the sorbents. Johnsen et al. [11] used the shrinking core model (SCM) to describe the CaO carbonation kinetics. Nikulshina et al. [27] chose the unreacted kinetic model (UKM) to precisely describe the capturing of CO_2 over CaO. Lee et al. [19] used TGA to examine the carbonation conversion data over the temperature range of 923 – 1023 K. Rodríguez et al. [28] reported a first order carbonation kinetics for the capture of CO_2 given in **Appendix-A2**. The sorption of CO_2 over LZC is a highly exothermic reaction as indicated in R8.

$$Li_2ZrO_{3(s)} + CO_{2(g)} \rightarrow Li_2CO_{3(s)} + ZrO_{2(s)} \qquad \Delta H^0_{298K} = -160 kJmol^{-1}_{Li_2ZrO_3} \tag{R8}$$

Ida et al. [29] found the CO_2 sorption kinetics in LZC by using double shell unreacted core model. Ochoa-Fernández et al. [25] studied the properties of CO_2 capture over LZC. They used the extent of reaction (x) to describe the CO_2 capture properties over LZC. Their proposed kinetics are used in this work and the rate equations are given in **Appendix-A3**.

LZC has the ability to hold water and it also displays increased chemisorption kinetics under wet conditions [30]. Steam is also reported to enhance CO_2 diffusion through the layer of carbonate formed over LZC [30]. However, it does cause a continuous deactivation, lowering the capacity of the acceptor due to phase segregation, sintering or vaporization of alkali metals after forming hydro-oxides in the presence of steam. Capture kinetics, regeneration and stability of LZC under steam conditions showed that capture kinetics were considerably improved with 10% steam concentrations [31].

K – HTC shows a chemisorption of CO_2 over the fresh sorbent followed by reversible and weak physical sorption. The sorption of CO_2 over HTC is slightly exothermic with $\Delta H^0_{298K} = -17$ kJ mol^{-1}_{K-HTC}. Ding et al. [24] used Langmuir model to adequately describe the CO_2 sorption kinetics by using both dry and wet feed conditions. The linear driving force (LDF) model was found to be feasible for describing the intraparticle mass transfer process during carbonation reaction. The kinetic model of HTC along with effective mass transfer coefficient, Langmuir model parameter, and LDF model is presented in **Appendix-A4**. The CO_2 adsorption capacity in dry condition is always lower than in wet condition. This suggests that the presence of water vapors is able to further activate adsorption sites, possibly by maintaining the hydroxyl concentration of the surface, and/or preventing site poisoning through carbonate or coke deposition [32].

2.2. Model development and its essential features

To illustrate the physical and chemical behavior, 1-dimensional heterogeneous model is adapted from [13] for the SE-SMR process with the different sorbents. To summarize, the original model describes mass and energy balance equations that account for both solid and gas phases and is formulated dynamically due to the time-dependent nature of sorption reaction (R4). The flow of gases in a reactor is assumed essentially ideal plug flow in nature while the direction of flow of gases is supposed to be only in axial direction. Peclet number Pe = uL/D_e) is considered to be greater than 800, hence, the mixing of gases and variation of temperature and concentration across the radial direction of packed bed reactor can be neglected. In order to take the advantage of the exothermic nature of the sorption reaction (R4), an adiabatic behavior of packed bed reactor is assumed. Fernandez et al. [3] suggested that the adiabatic SE-SMR reactor gives a shorter pre-breakthrough period as compared to non-adiabatic (quasi-isothermal) reactor. The adiabatic process also enhanced the energy efficiency of the reactor and it eliminated the need for heat transfer equipment for SE-SMR process [3]. Only CO_2 is considered to be adsorbed on the surface of sorbent. Ideal gas behavior of gases, uniform size of the catalyst and sorbent throughout the reactor, and constant packed bed porosity is also assumed. Fig. 1 shows the essential features of the mathematical model. The reforming and carbonation stage of the SE-SMR process is limited by mass transfer, in particular diffusion of the intermediary and final products between the catalytic and sorption sites. The single combined particle system greatly minimizes the effective diffusion distance and prevents dilution of intermediates by the bulk gas, thereby promoting improved mass transfer rates and conversion efficiencies [33, 34]. The mass diffusion fluxes can be described according to the Maxwell–Stefan.

Low temperatures in SE-SMR result in lack of H_2 production and it favours the Boudouard carbon formation reaction (R9) but at the same time elevated temperatures aid in coke oxidation by steam [35].

$$2CO_{(g)} \leftrightarrow CO_{2(g)} + C_{(s)} \qquad \Delta H^0_{298K} = -172.5 \quad kJ \quad mol^{-1}_{CO} \tag{R9}$$

Excess supply of steam suppresses the coke formation by shifting R1 towards more H_2 production and also according to Dou et al. [36], the Boudouard reaction is not dominant even at the temperature of 500 °C because of the low ratio of CO/CO_2. In one of our recent work [37], we have investigated the equilibrium coke formation for SE-SMR and it was observed that coke deposition becomes less intense as S/C approaches 1. Thus, if a sufficiently high enough S/C ratio is provided then the undesired carbon formation can be suppressed. In our present work, S/C of 3 is chosen, thus coke formation has not been taken into account as an equilibrium product to perform the analysis. The parameters and operating conditions used during the modeling of the SE-SMR reactor are tabulated in Table 1.

Table 2 illustrates the mass and energy balances for component 'i' (i = CH_4, CO, CO_2, H_2, and H_2O) in both gas and solid phase. Where 'ε_b', 'ρ_g', 'C_{pg}' and 'η_j' correspond to the bed porosity, density, specific heat of gases and effectiveness factor respectively. In the current model, $\eta_j$is assumed equal to 1.0 by neglecting diffusion resistance between gas and solid phases. Effect of the variation of temperature is also incorporated in the heat capacity of gases. The pressure drop in the bed of the reactor is modified by using Ergun's equation. The equations regarding calculations of physical properties like thermal conductivities, mass and heat transfer coefficient along with the dimensionless numbers are presented in **Appendix-B**. To solve these equations, initial and boundary conditions are listed in **Appendix-C1**. At the start of the reactor, initial concentration (C_i) should be set to zero, but this will make the SMR rates infinity. To avoid this problem, a very small initial concentration is set for H_2.

The model is implemented in gPROMS for the solution of the equations. To solve partial differential equations included in this model, a first order backward finite difference method (BFDM) was used. The reactor length (L) was discretized into 100 uniform intervals and results were reported after every 10 s

3. Results and discussion

3.1. Model validation

In our previous work [13], the SE-SMR process in an adiabatic packed bed reactor using CaO as the sorbent is validated against the

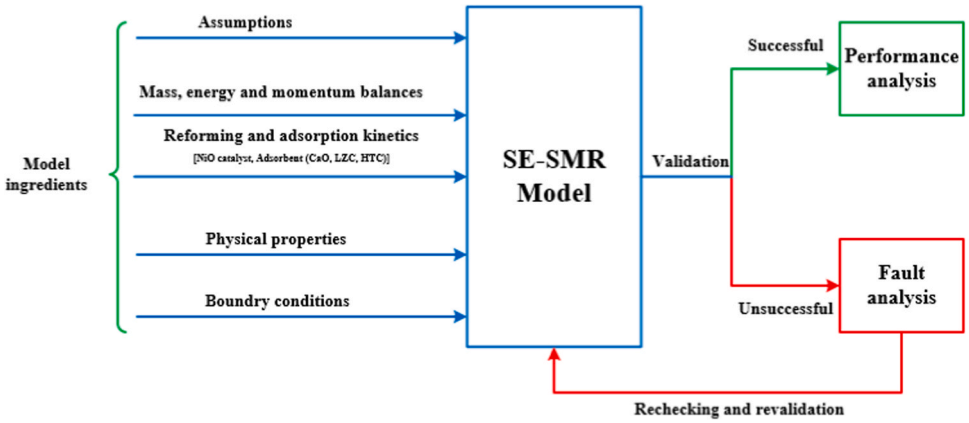

Fig. 1. Essential ingredients of the mathematical model.

Table 1
The parameters and operating conditions used in the modeling of SE-SMR reactor.

Reactor bed characteristics and operating conditions	Value
Density of catalyst, ρ_{cat} [kg m^{-3}]	550
Density of bed, ρ_{bed} [kg m^{-3}]	1625
Specific heat of bed, $C_{p,bed}$ [J kg^{-1} K^{-1}]	980
Average gas viscosity, μ [kg m^{-1} s^{-1}]	1.8×10^{-4}
Steam to carbon ratio, S/C [-]	3
Particle diameter, d_p [m]	0.01
Bed porosity, ε_b [-]	0.5
Reactor length, L [m]	7
CaO density, $\rho_{ads,CaO}$ [kg m^{-3}]	1125
LZC density, $\rho_{ads,LZC}$ [kg m^{-3}]	596
HTC density, $\rho_{ads,HTC}$ [kg m^{-3}]	1300
Catalyst/sorbent ratio	0.35

Table 2
Effect of temperature on CH_4 conversion, H_2 yield (wt%), H_2 purity and CO_2 capture efficiency at 5 bar, S/C of 3.0 and 0.5 kg m^{-2} s^{-1} using HTC.

Temperature [K]	CH_4 conversion [x_{CH4}, %]	H_2 Yield $= \frac{n_{H2,out}}{n_{H2,stoic}}$	H_2 purity [%]	CO_2 capturing efficiency [%]
673	21.60	0.67	45.55	20.03
693	27.56	0.85	53.38	25.65
713	33.86	1.04	60.39	31.59
733	39.94	1.23	66.19	37.17
753	46.72	1.44	71.78	43.48
773	55.18	1.69	77.81	51.75
793	60.83	1.87	81.12	56.50
813	67.88	2.08	84.90	62.95
833	74.64	2.29	88.11	69.09
853	80.86	2.48	90.74	74.71
873	86.27	2.64	92.82	79.57

outcomes of chemical equilibrium and applications (CEA) software and literature data. CEA software is based on minimization of Gibbs free energy (G) [38]. To study the performance of SE-SMR process, we used the industrial conditions for temperature, pressure and S/C. In the current work, we are using the same validated model to understand the performance of SE-SMR reactor under the low-pressure conditions (3 – 11 bar) by using different (CaO, LZC and HTC) sorbents. The extent of reaction (x) of CO_2 sorption using LZC as the CO_2 sorbent is simulated and validated against the experimental outcomes of Ochoa-Fernández et al. [25]. Fig. 2 shows the dynamic variation in the extent of reaction at various partial pressures of CO_2 (0.5, 0.7 and 1 bar) and a temperature of 848 K. Ochoa-Fernández et al. [25] studied the extent of reaction at various partial pressures of CO_2 and two temperatures (823 K and 848 K). Here, validation of model outputs against the literature is performed at 848 K owing to the higher activity of sorbent, which helps it in reaching saturation more quickly as compared to 823 K and fast cyclic operation can be performed. The values for kinetic parameters (k_{ad}, E_{ad}, T_o, and n) are taken from the literature and presented in **Appendix A-3** [25]. At high p_{CO_2} (1 bar), the LZC sorbent approaches its saturation point quickly as compared to low values of p_{CO_2} because of the CO_2 sorption on LZC is favored under high-pressure conditions. There is an excellent agreement observed between the modeling outputs and the experimental results available in the literature.

At 150 s, the simulated extent of reaction (x_M) for $p_{CO_2} = 1$ bar is 0.673 ($uptake_{CO2}$/maximum $uptake_{CO2}$), whereas experimental extent of reaction (x_E) at 150 s is 0.707. Similarly, the experimental and modeling data for the extent of reaction at $p_{CO_2} = 0.7$ bar and 270 s is 0.670 and 0.671 respectively. At $p_{CO_2} = 0.5$ bar, x_E and x_M curves are less sharp and large time is required to saturate the LZC sorbent because the kinetics of LZC reported by Ochoa-Fernández et al. [25] is of second order. They reported complex mechanism for CO_2 sorption on LZC and modeling equations that were used to describe the CO_2 sorption experimentally indicated a second order reaction.

The kinetics of HTC **(Appendix A-4)** used in this study are first validated by using the experimental data of Ding et al. [24]. The model is validated under both dry and wet feed conditions. The steam is used as reactant in the SE-SMR process, hence, only wet feed conditions are discussed in this work under the operating conditions of 673 K and 753 K. Fig. 3 shows the effect of p_{CO2} (0 – 0.45 bar) on the sorption

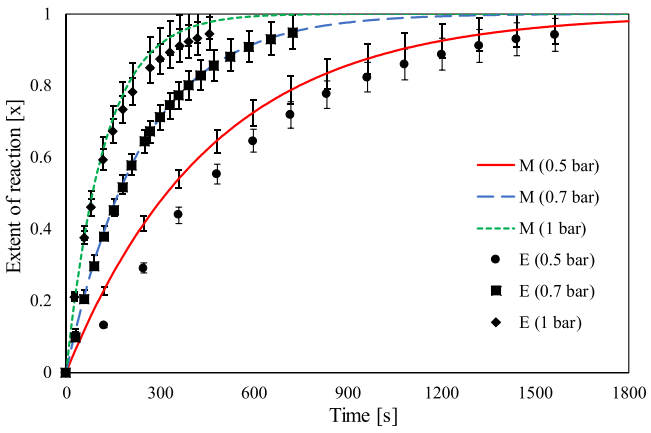

Fig. 2. Comparison of experimental and simulated extent of reaction (x) of CO_2 sorption by using LZC at 848 K and 0.5–1 bar. Dots are the experimental data and solid lines represent the outputs of modeling work conducted in this work.

capacity of HTC at 673 K and 753 K. The values of parameters like pore diffusion coefficient (D_p), reference temperature (T_o) and heat of sorption (ΔH_{ads}), used in the model were taken from the literature [24]. The value of ΔH_{ads} is − 10 kJ mol^{-1} and − 17 kJ mol^{-1} for the dry and wet feed conditions respectively.

It can be seen in Fig. 3 that both Langmuir isotherm curves show a sudden rise for 0 – 0.1 bar, which illustrates that sorption capacity of HTC is increased as the p_{CO_2} is increased from 0 to 0.1 bar. At 673 K, Langmuir parameter ($b_{CO_2,ref}$) is 23.6 bar^{-1} and maximum sorption capacity (0.65 mol_{CO2}/kg_{HTC}) is used. At 673 K and 0.2 bar, the modeling and experimental value of sorption capacity is 0.536 and 0.539 mol_{CO2}/kg_{HTC} respectively. At 753 K and 0.2 bar p_{CO_2}, the modeling and experimental value of sorption capacity is 0.460 and 0.458 mol_{CO2}/kg_{HTC} respectively. An excellent agreement is observed between the modeling and experimental values of sorption isotherm.

3.2. Methodology of thermodynamic analysis

An independent equilibrium-based software, CEA by NASA [39,40], is used to calculate the thermodynamic equilibrium composition of product gases as a function of changes in temperature and pressure. These compositions are then employed to calculate CH_4 conversion (%), H_2 purity (%), H_2 yield (%) and CO_2 capture efficiency (%) at equilibrium by using Eqs. (6–9) respectively. The CEA is based on minimization of Gibbs free energy. In this study, the chemical equilibrium of the SE-SMR process is calculated for CaO and LZC sorbents by specifying the different conditions of temperature, pressure, and S/C. The thermodynamic data (enthalpy, entropy, heat capacity and heat of formation) for LZC is taken from the literature [41,42] and are inserted in the CEA database. The species CH_4, CO, CO_2, H_2, H_2O, N_2, CaO, and $Ca(OH)_2$ are added in the CEA software for performing the estimations. N_2 is essentially incorporated to calculate the total moles at the outlet. The 'only' command (option integrated into the software suite) is used to specify the possible products obtained from the SE-SMR process. The effect of temperature and pressure is studied by considering the reactor system at isobaric and isothermal conditions respectively with a fixed S/C, while the effect of S/C is analyzed at equilibrium by keeping both pressure and temperature constant. In this way, optimum values of reactor's operational parameters at equilibrium are unveiled.

3.3. Analysis of temperature profile

The adsorption of CO_2 over sorbents is exothermic. This nature of sorption reaction (R4) causes a rise in the temperature of the SE-SMR process from its initial (feed) temperature, depending on the quantity of heat (ΔH_{ads}) released by the sorbent. This rise in temperature will give

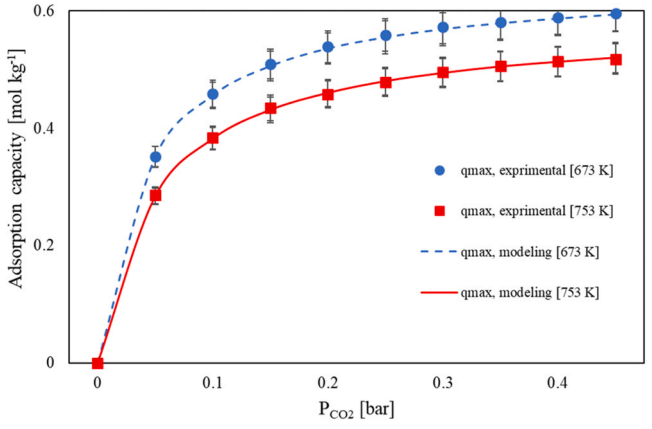

Fig. 3. The effect of CO_2 partial pressure on the sorption capacity (mol kg^{-1}) of HTC under different temperature (673 and 753 K) conditions. Dots are the experimental data and solid lines are the outputs of the current modeling work.

a transient temperature profile inside the reactor for different sorbents. Fig. 4 (a–c) shows the transient temperature profiles of the SE-SMR process using CaO, LZC and HTC as sorbents. Fig. 4 (a) presents the temperature profile, at the exit of the reactor, using CaO as a CO_2 sorbent at 900 K, 3 bar, S/C of 3.0 and G_s of 3.5 $kgm^{-2}s^{-1}$. During the initial stages (t = 0 – 200 s), the temperature profile is almost steady. The heat supplied by the exothermic sorption reaction (R4) is fully utilized by the endothermic SMR reactions (R1 and R2), hence, a steady uniform linear temperature profile is observed. Since the overall SE-SMR process, using CaO is slightly exothermic (ΔH^0_{298K} = − 13.9 kJ mol^{-1}_{CaO}), two peaks can be observed in the temperature profile (Fig. 4 (a)). The first rise in the temperature shows fast sorption at t = 200 s. According to the Le Chatelier's principle, this rapid sorption of CO_2 enhances the CH_4 conversion and produces more H_2 and CO_2 at the outlet of the reactor. The more sorption of CO_2 results in continued rise in the temperature profile as can be seen from 280 to 690 s (pre-breakthrough period). Once the sorbent is fully saturated, a sharp decrease in the temperature profile is observed from 690 to 910 s (breakthrough period). After the breakthrough period (t > 910 s), the SE-SMR process behaves similarly to the SMR process as no CO_2 sorption is taking place and only the reforming (R1 and R2) and shift (R3) reactions are occurring within the reactor. The cut-off for the reactor bed should be somewhere in the pre-breakthrough region where the optimal CH_4 conversion is achieved along with the optimal H_2 purity. It is actually the tradeoff between the overall CO_2 sorbent capacities used during the SE-SMR process and the optimal H_2 purity and CH_4 conversion achieved. Fernandez et al. [3] found the rise in temperature (ΔT_{rise} = T_{max} − T_{feed}) during the SE-SMR process to be 32 K. In this study, ΔT_{rise} is 17.5 K. The low ΔT_{rise} is because the endothermic SMR process favors low pressure as described earlier. As a result, high CH_4 conversion (%) is achieved at low-pressure conditions. CaO is highly hydroscopic and below 400 °C it undergoes CaO hydration reaction (R10) which is a highly exothermic reaction (ΔH^0_{298K} = − 218.4 kJ mol^{-1}_{CaO}). This reaction further proceed towards $Ca(OH)_2$ carbonation reaction (R11). The hydration of sorbent occurs well below the temperature under consideration in this paper. The regeneration of the carbonated sorbent is highly endothermic reaction and occurs at high temperature (850–1000 °C) under atmospheric pressure. The temperature conditions studied in this paper are well below the temperature condition under which calcination or decomposition of CaCO3 occurs. Therefore, these reactionS (CaO hydration and $CaCO_3$ decomposition) have not been considered in this work.

$$CaO_{(s)} + H_2O_{(g)} \rightarrow Ca(OH)_{2(s)} \qquad \Delta H^0_{298K} = -218.4 kJmol^{-1}_{CaO} \qquad (R10)$$

$$Ca(OH)_{2(s)} + CO_{2(g)} \rightarrow CaCO_{3(s)} + H_2O_{(g)} \qquad \Delta H^0_{298K} = -64.14 kJmol^{-1} \qquad (R11)$$

The temperature profile for LZC and HTC is shown in Fig. 4 (b) and (c), respectively. The pre-breakthrough period for LZC (t < 250 s) is much shorter than the pre-breakthrough period in case of CaO (t < 690 s). This indicates the low sorption capacity of LZC (5.0 $mol_{CO2} kg^{-1}_{sorbent}$) with relation to CaO (16.3 $mol_{CO2} kg^{-1}_{sorbent}$). The breakthrough period for LZC is last by 1870 s, and the ΔT_{rise} for LZC is 20 K as compared to 17.5 K in the case of CaO. The temperature profile is entirely different when HTC is used to uptake CO_2. There was no appreciable rise in the temperature observed for the HTC because of its low heat of adsorption (ΔH^0_{298K} = − 15 kJ mol^{-1}_{K-HTC}). The overall SE-SMR process using HTC remains endothermic in nature. During the period t < 500 s, there is a steady decrease in time-dependent temperature profile at the outlet of the reactor. A sharp decrease in temperature of 42 K is observed for the period 500 – 1400 s, which is followed by a slight rise of 7 K in temperature during the period 1400–2000 s, and this rise is due to the smaller value of heat of sorption for HTC.

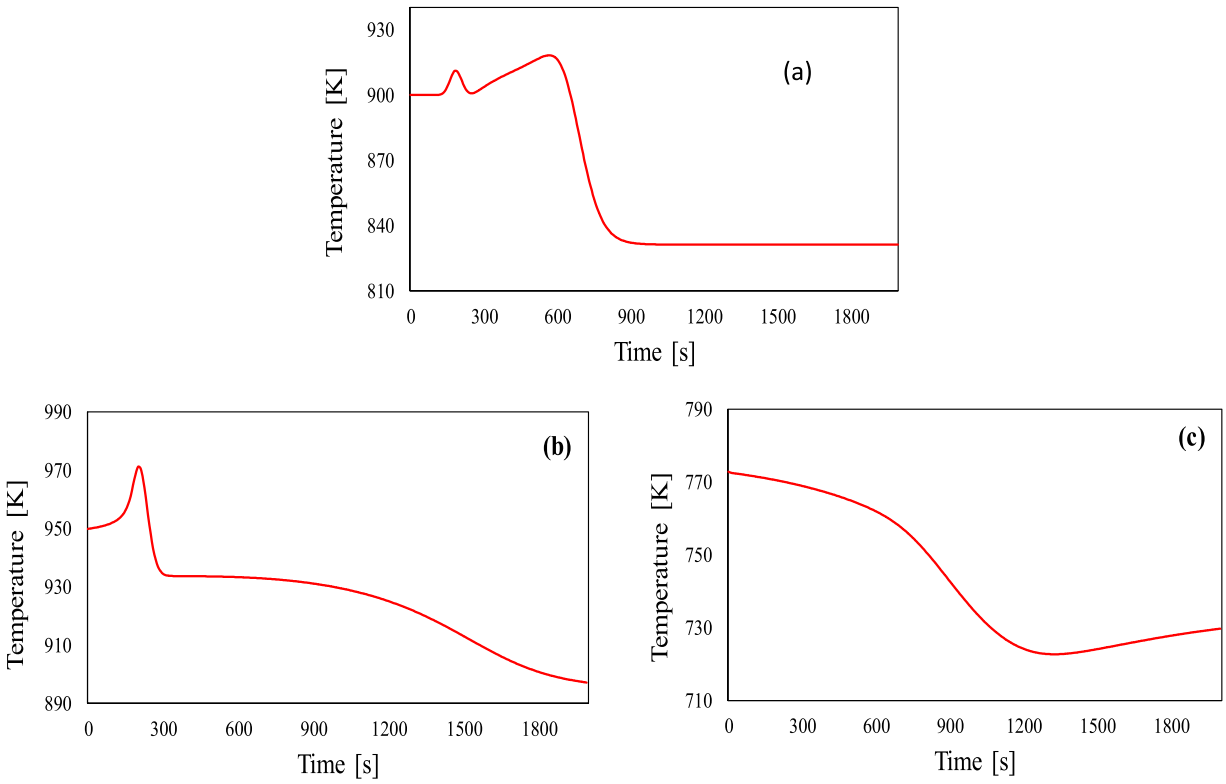

Fig. 4. Temperature profiles of (a) CaO at 900 K, 3 bar, S/C of 3.0, and G_s of 3.5 kg m^{-2} s^{-1}, (b) LZC at 950 K, 10 bar, S/C of 3.0 and G_s of 2.5 kg m^{-2} s^{-1} and (c) HTC at 773 K, 5 bar, S/C of 3.0 and G_s of 0.5 kg m^{-2} s^{-1}.

3.4. Sensitivity analysis

3.4.1. Effect of temperature

The conventional SMR process is operated in fertilizer industries over the range of 1073 – 1273 K and 20 – 35 bar. Since sorption of CO_2 and SMR are temperature sensitive processes, the variation in temperature has a robust influence in the performance of the overall SE-SMR process. Fig. 5 illustrates the performance of the reactor in terms of CH_4 conversion, H_2 yield, H_2 purity, CO_2 capture efficiency with CaO as a sorbent. The following equations were used to calculate the CH_4 conversion, H_2 purity and CO_2 capture efficiency [43] while H_2 yield is calculated as moles of H_2 produced per mole of CH_4 [44]. H_2 yield can

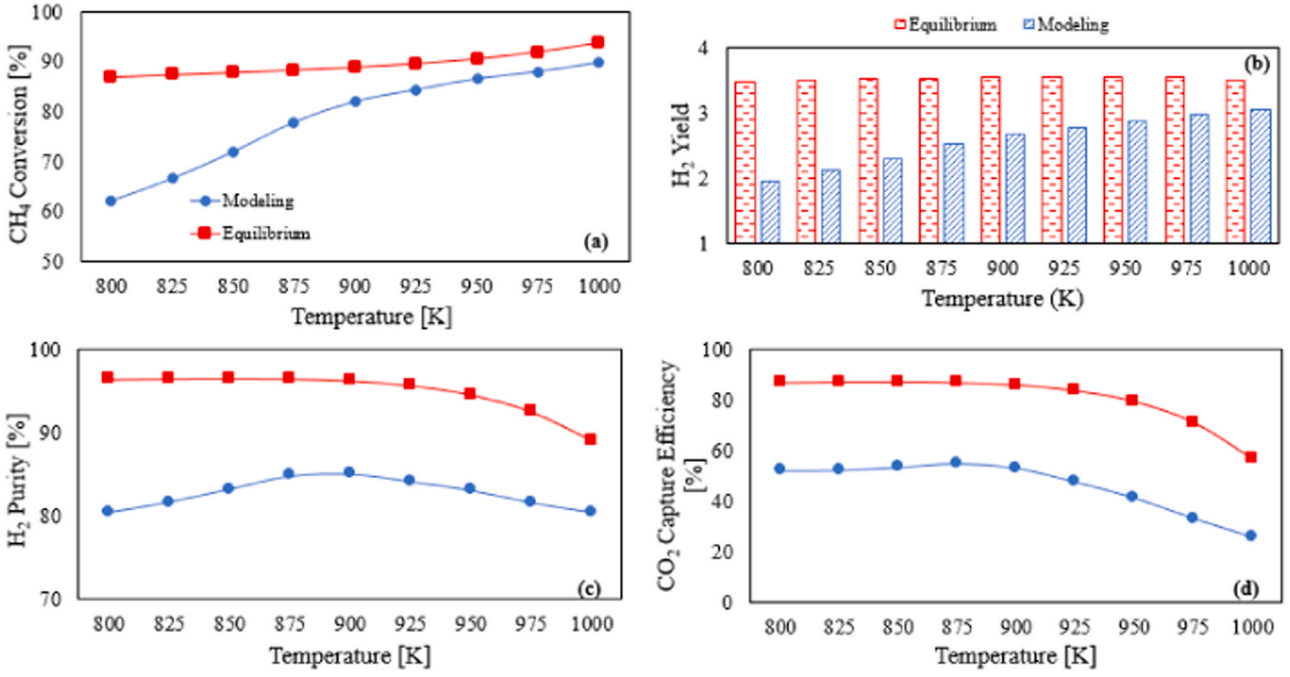

Fig. 5. The effect of temperature on (a) CH_4 conversion (%), (b) H_2 yield, (c) H_2 purity (%) and (d) CO_2 capture efficiency (%) at 3 bar, S/C of 3.0 and 3.5 kg m^{-2} s^{-1} by using CaO sorbent.

also be defined as moles of H_2 produced divided by the stoichiometric amount of produced H_2 by the reforming reaction, which is 4 moles of H_2 per mole of CH_4 [43].

$$CH_4 \quad \text{Conversion} \quad [\%] = \frac{(n_{CH4.in} - n_{CH4,out})}{n_{CH4,in}} \times 100 \tag{6}$$

$$H_2 \quad \text{Purity} \quad [\%] = \frac{n_{H2,out}}{(n_{H2,out} + n_{CH4,out} + n_{CO,out} + n_{CO2,out})} \times 100 \tag{7}$$

$$H_2 \quad \text{Yield} \quad (\text{wt.} \quad \% \quad \text{of} \quad CH_4) = \frac{MW_{H2} \times n_{H2,out}}{MW_{H2} \quad \times n_{CH4,in}} \times 100 \tag{8a}$$

$$H_2 \quad \text{Yield} \quad = \frac{n_{H2,out}}{n_{H2,stoic}} \tag{8b}$$

$$CO_2 \quad \text{Capture} \quad [\% \quad] = \frac{(n_{CH4.in} - n_{CH4,out} - n_{CO,out} - n_{CO2,out})}{n_{CH4,in}} \times 100 \tag{9}$$

The effect of temperature on CH_4 conversion at 3.5 $kgm^{-2}s^{-1}$, 3 bar and with a S/C of 3 is depicted in Fig. 5 **(a)**. At 800 K, the simulated CH_4 conversion (62.1%) is much lower as compared to the equilibrium results (86.9%) generated via CEA software as the SMR kinetics are not favorable at such low temperature (800 K). As, the temperature increases from 800 to 1000 K, the CH_4 conversion increases from 62.2% to 89.8% and 86.9 – 93.6% for the case of simulation and equilibrium respectively.

It is evident from Fig. 5 that at 900 K, the simulation provides values of 85% and 55% related with H_2 purity and CO_2 capture efficiency respectively. While the equilibrium values of H_2 purity and CO_2 uptake efficiency under the same temperature are 96.2% and 85.9% respectively. At 1000 K, the simulation results reveal a CH_4 conversion of 89.7% whilst the H_2 purity is 80.3% (a slight decrease). This can be associated with the very low CO_2 capture efficiency (25.4%) experienced at such a high temperature. The low CO_2 capture efficiency at 1000 K is mainly due to the ineffectiveness of the carbonation reaction (R6) at such a high temperature and it is explained further in Fig. 6.

Fig. 6 shows the effect of temperature on the rate of carbonation (r_{ads}) at 800 – 1000 K using CaO sorbent. The rate of carbonation increases as the temperature increases from 800 to 950 K. This shows the increase in temperature results in more uptake of CO_2 on the active sites of CaO sorbent. After 950 K, the r_{ads} decreases. At 800 K, the peak value for r_{ads} is 6.8×10^{-3} mol $kg^{-1}s^{-1}$ as compared to 13.6×10^{-3} and 15.4×10^{-3}mol $kg^{-1}s^{-1}$ for 900 and 950 K respectively. The pre-breakthrough point at 800 K and 950 K is 780 s and 730 s respectively. This shows that CaO saturates quickly at 950 K than at 800 K.

Fig. 7 shows the effect of temperature on CH_4 conversion, H_2 purity, H_2 yield and CO_2 capture efficiency at 10 bar and 3.5 $kgm^{-2}s^{-1}$ by using

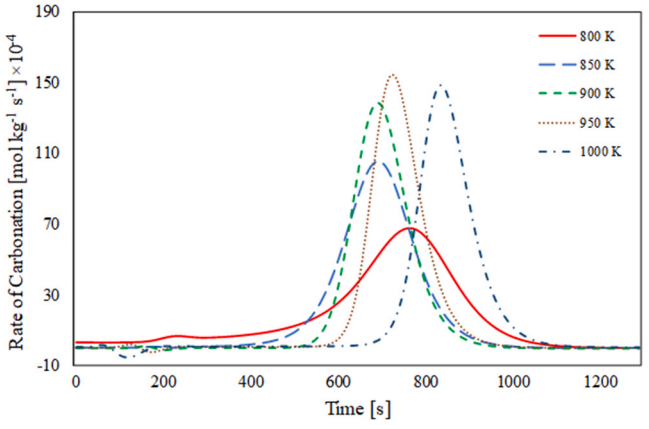

Fig. 6. The dynamic effect of temperature on the rate of carbonation ($mol_{CO2}/kg_{sorbent}$) of CaO sorbent at 3 bar, 3.5 kg m^{-2} s^{-1} and S/C of 3.0.

LZC. The CH_4 conversion increases with the increase in temperature at 950 K and S/C of 3, 91.2% and 94% CH_4 conversion is achieved in the case of modeling and equilibrium results respectively. At 975 K, H_2 purity reaches its maximum value of 95.5% while CO_2 capture efficiency has its peak value of 86.7%. As temperature increases from 975 to 1000 K, the H_2 purity and CO_2 uptake efficiency decrease to 94.75% and 83.8% respectively.

Reijers et al. [45] performed the experiments to study the effect of temperature on the adsorption capacity of htc-based materials. They concluded that the adsorbing capacity decreases as the temperature increases beyond 673 K. According to Pérez-Ramírez et al. [46], HTC-like compounds follow a two-step decomposition behaviour. The first step is the removal of interlayer water molecules at a temperature well below 500 K (dehydration step). In the second step, the collapse of the positively charged brucite-like layers with interlayer space occupied by charge compensating anions and water molecules occurs in the temperature range of 500–773 K. In this temperature range, the decomposition of CO_3^{2-} in the interlayer occurs and the material is dehydrated by the dehydroxylation of the brucite-like sheets, although this decomposed material still has the capability of adsorbing CO_2 at this temperature (dihydroxylation and decarbonation step). Hutson et al. [47] observed the transition of the material to a solid solution of magnesium and aluminium oxides at 873 K, which results in the release of O_2 and final transition to a spinel at 1173 K. Above 873 K, the ability to effectively adsorb CO_2 is lost and this limits the use of HTC-based materials in the range 673–873 K. Due to this limitation associated with HTC, a temperature range of 673 – 873 K is selected to study the effect of temperature on CH_4 conversion H_2 yield and purity, and CO_2 capture efficiency. Above 873 K, HTC-based materials are decomposed and no longer act as a sorbent but can be used instead as a reforming catalyst support. This problem limits the use of HTC-based materials as sorbents in a narrow temperature range otherwise they have the potential to give excellent results at high temperatures.

Table 2 illustrates the effect of temperature on CH_4 conversion H_2 yield and purity, and CO_2 capture efficiency using HTC at 5 bar, G_s of 0.5 kg m^{-2} s^{-1} and S/C of 3. CH_4 conversion and H_2 yield increases continuously as the temperature increases from 673 to 873 K. H_2 purity increases from 45.5% to 92.8% as the temperature increases from 673 K to 873 K. The rise in H_2 purity is due to the increase in CO_2 capture efficiency as can be seen in Table 2.

The selection of an optimum temperature depends upon the overall performance of the sorbent in terms of CH_4 conversion; H_2 yield, H_2 purity and CO_2 capture efficiency. Based on the results presented so far and due to the decomposition problems associated with HTC at elevated temperatures, 773 K is selected as an optimum temperature for HTC sorbent, whilst 900 K and 950 K provided the best performance in the case of the CaO and LZC sorbents, respectively.

3.4.2. *Effect of pressure*

A lot of work has been done in the literature to investigate the performance of SE-SMR process under the high-pressure conditions (20–40 bar) [3,11,13]. Since SMR operation is favorable at low pressures, it could be valuable to test SE-SMR model close to atmospheric conditions as high-pressure conditions give rise to low H_2 purity and CH_4 conversion. Kwang et al. [9] tested calcined arctic dolomite at low-pressure conditions (1 – 5 bar) and obtained 95% purity of H_2 (dry basis). The current model of SE-SMR is developed and simulated under low-pressure conditions (3 – 11 bar) to find the best operating conditions for CaO, LZC and HTC sorbents.

In the previous section, optimum temperatures were selected for CaO, LZC and HTC. Bearing in mind these optimum temperatures, the most favorable pressures in the range of 3–11 bar are investigated. Fig. 8 presents the performance experienced by CaO, LZC and HTC in terms of CH_4 conversion, H_2 yield, H_2 purity and CO_2 capture efficiency. Fig. 8 (a) shows the effect of pressure on the performance of SE-SMR process using CaO as sorbent at 900 K, S/C of 3 and G_s of 3.5 kg $m^{-2}s^{-1}$. The

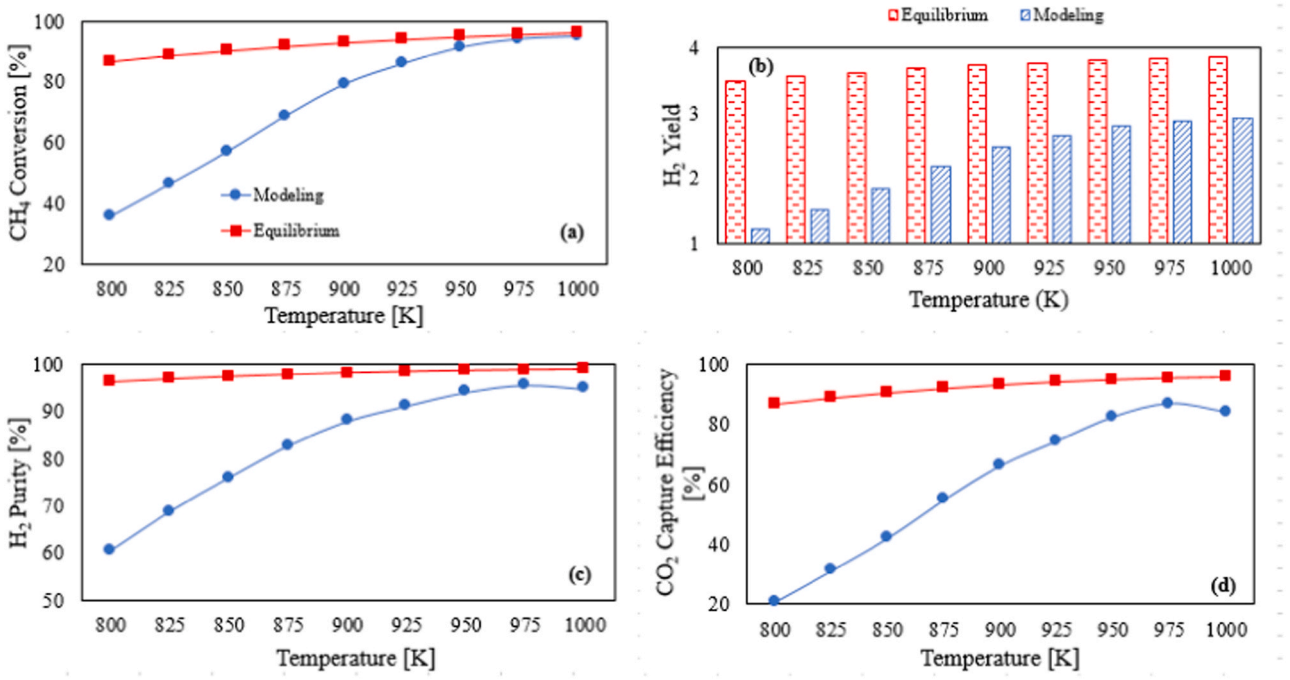

Fig. 7. The effect of temperature on (a) CH_4 conversion, (b) H_2 yield, (c) H_2 purity (%) and (d) CO_2 capture efficiency at 10 bar, S/C of 3.0 and 2.5 kg m^{-2} s^{-1} by using LZC as a CO_2 sorbent.

pressure has a negative effect on the CH_4 conversion and H_2 yield, whereas the CO_2 capture efficiency increases as the pressure increases. This is because the carbonation kinetics used in this model is favored at relatively high pressures. Using CaO as a sorbent gives 81.98% CH_4 conversion at 3 bar as compared to 71.54% at 10 bar. H_2 purity decreases from 85.02% to 84.15% as pressure increases from 3 to 4 bar. The decrease in H_2 purity is due to the decrease in the CH_4 conversion from 81.98% to 76.56% as pressure increases from 3 to 4 bar. After

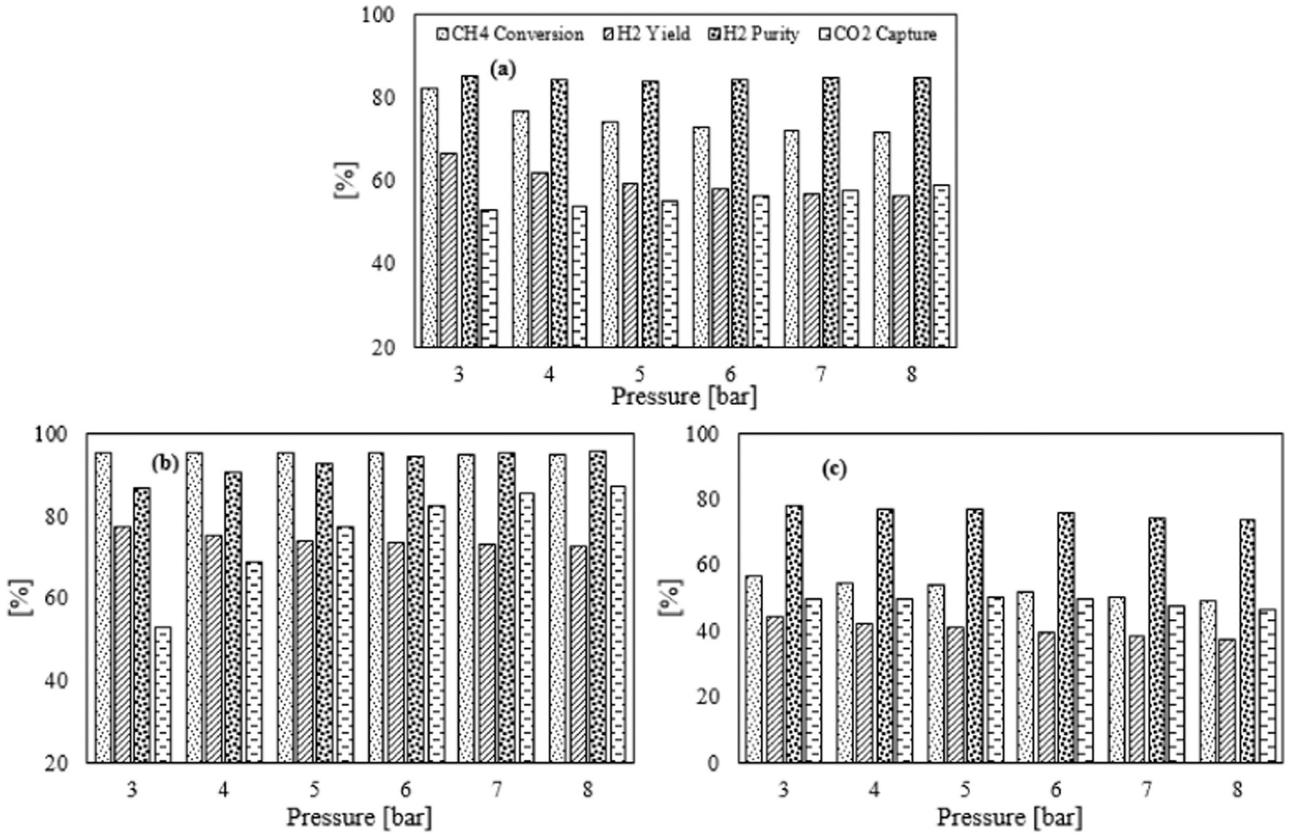

Fig. 8. The effect of pressure on CH_4 conversion, H_2 yield, H_2 purity and CO_2 capture efficiency using (a) CaO, (b) LZC and (c) HTC at the optimum temperatures, S/C of 3.0 and sorbent/carbon of 1.

4 bar, H_2 purity almost remains steady due to a slight increase in CO_2 capture efficiency.

CH_4 conversion and H_2 yield for LZC and HTC decrease by increasing the feed pressure because the kinetics of the SMR process are not favorable at high pressure. The decrease in CH_4 conversion with the increase in pressure results in a decrease in H_2 yield. The LZC sorbent gives maximum CH_4 conversion and H_2 yield up to 95.07% and 73.36% respectively at 6 bar. H_2 purity increases from 86.76% to 95.73% as pressure increases from 3 to 8 bar. The increase in H_2 purity with the increase in pressure is mainly due to the rise in CO_2 capture efficiency. Fig. 8 (c) shows the effect of pressure on SE-SMR process using HTC as a sorbent at 773 K and G_s of 0.5 $kgm^{-2}s^{-1}$. At 3 bar, the CH_4 conversion and H_2 yield has a value of 56.73% and 44.31% respectively. As the pressure increases from 3 to 8 bar, the CH_4 conversion decreases from 56.73% to 48.82%. In the case of HTC, a different trend is observed for both H_2 purity and CO_2 capture efficiency, as both approach their peak values at 5 bar. The outcomes showed thus far demonstrate that the optimum values of pressure for LZC and HTC are 10 bar and 5 bar respectively.

Fig. 9 (a–c) illustrates the effect of pressure on the rate of reforming (R1) and carbonation reaction for the three sorbents under consideration. A significant impact of pressure is observed on the CO_2 sorption because the rate of carbonation is strongly depended upon pressure conditions as reported in our previous work [13]. In Fig. 9 (a), the effect of pressure on the rate of reforming (r_{SMR}) and carbonation reactions (r_{ads}) using CaO is presented. Both r_{ads} and r_{SMR} decreases as the pressure increases from 3 to 6 bar. The r_{SMR} is approximately 4.5 times faster than r_{ads} at 3 bar. The maximum r_{ads} for CaO is found to be 13.6×10^{-4} mol $kg^{-1}s^{-1}$.

In Fig. 9 **(b)**, an entirely different trend is observed for LZC as both r_{ads} and r_{SMR} increase as the pressure increases from 9 to 12 bar. The r_{SMR} for LZC is 2.5 times faster than the r_{ads}. In regards to the r_{ads} for the CaO, is much faster than LZC and HTC at their optimum pressure conditions, which prove very fast kinetics of CaO as compared to LZC and HTC sorbents. The r_{ads} for HTC is higher at 7 bar than 4 bar, which means a superior CO_2 capture at 7 bar. The maximum r_{ads} for HTC at 4 bar is observed at 600 s whereas for 7 bar it is seen at 760 s

3.4.3. *Effect of mass flow velocity G_s*

Gs plays a vital role in the performance of the SE-SMR process. The value of G_s dictates the selection of the reactor length and cut-off time between sorption and desorption process. In theory, high values of G_s are favorable for shorter reactor length and fast cycling operations (sorption and desorption). Fig. 10 (a–c) shows the effect of G_s on H_2 and CO_2 composition (mole %, dry basis) at the outlet of the reactor for CaO, LZC and HTC sorbents.

Fig. 10 (a) shows the variation in CO_2 and H_2 concentrations during SE-SMR process using CaO sorbent at 900 K, 3 bar and S/C of 3. At low G_s, (2 kg m^{-2} s^{-1}), longer pre-breakthrough is observed (t = 1150 s). In Fig. 10 **(b)**, similar trend is observed using LZC sorbent. With the increase in G_s, pre-breakthrough period decreases with no significant effect on the molar concentration of H_2 and CO_2 at the outlet of the reactor. In case of CaO as sorbent, the pre-breakthrough period decreases from 1150 to 550s as G_s increases from 2 kg m^{-2} s^{-1} to 4 kg m^{-2} s^{-1}. The G_s of 3.5 kg m^{-2} s^{-1} is selected as optimum velocity for CaO sorbent and this gives 81.98% and 85.02% CH_4 conversion and H_2 purity respectively.

Fig. 10 (c) shows a significant change in the pre-breakthrough curve for the HTC sorbent. Here, a considerable change is observed in CH_4 conversion and H_2 purity by changing the G_s. This change is not prominent in the case of CaO as the kinetics of CaO sorbent are fast and do not vary much by the changing the G_s. The kinetics of HTC sorbent are slow, which means a long residence time is required to achieve high CH_4 conversion and H_2 purity. That is why, the optimum G_s for HTC

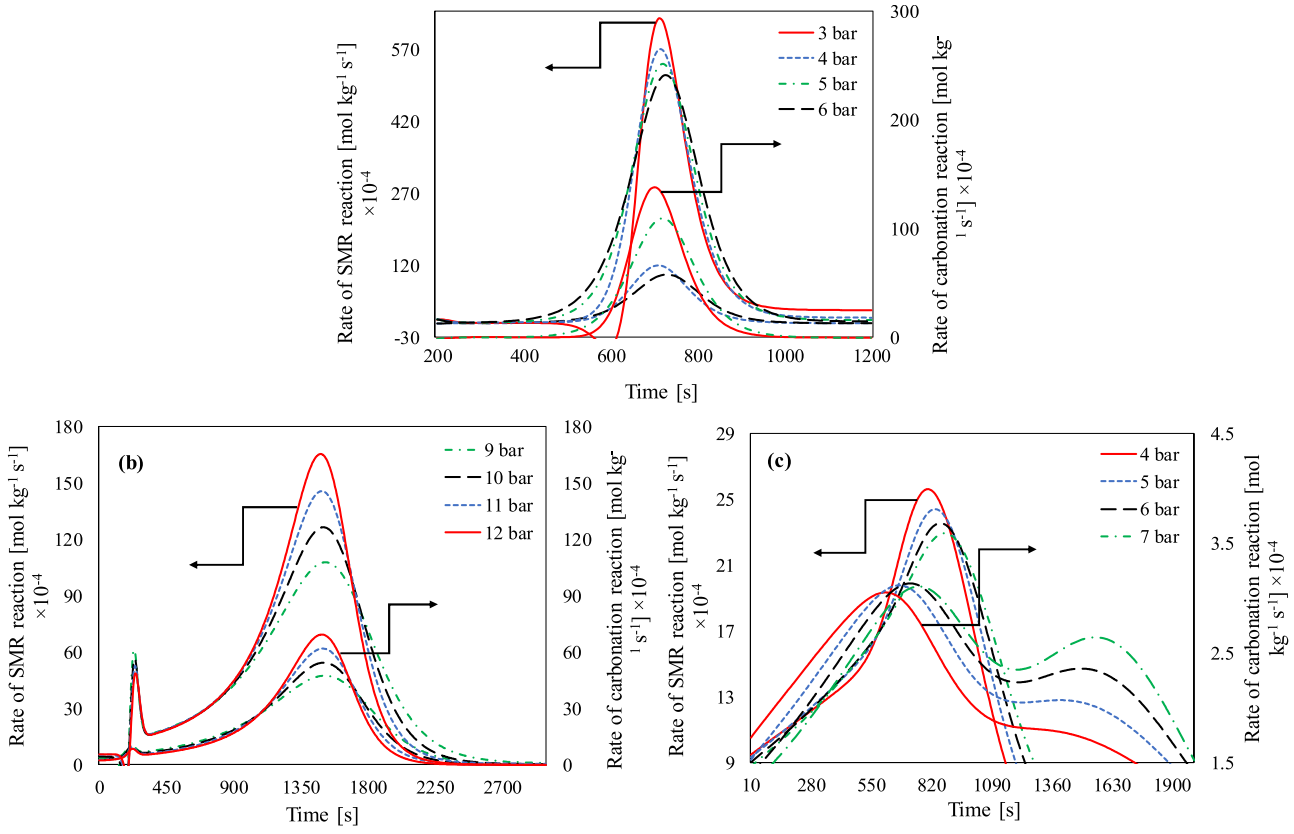

Fig. 9. The effect of pressure on the rate of SMR reaction (R1) and rate of carbonation by using (a) CaO at 900 K, S/C of 3.0 and G_s of 3.5 kg m^{-2} s^{-1}, (b) LZC at 950 K, S/C of 3.0 and G_s of 2.5 kg m^{-2} s^{-1} and (c) HTC at 773 K, S/C of 3.0 and G_s of 0.5 $kgm^{-2}s^{-1}$.

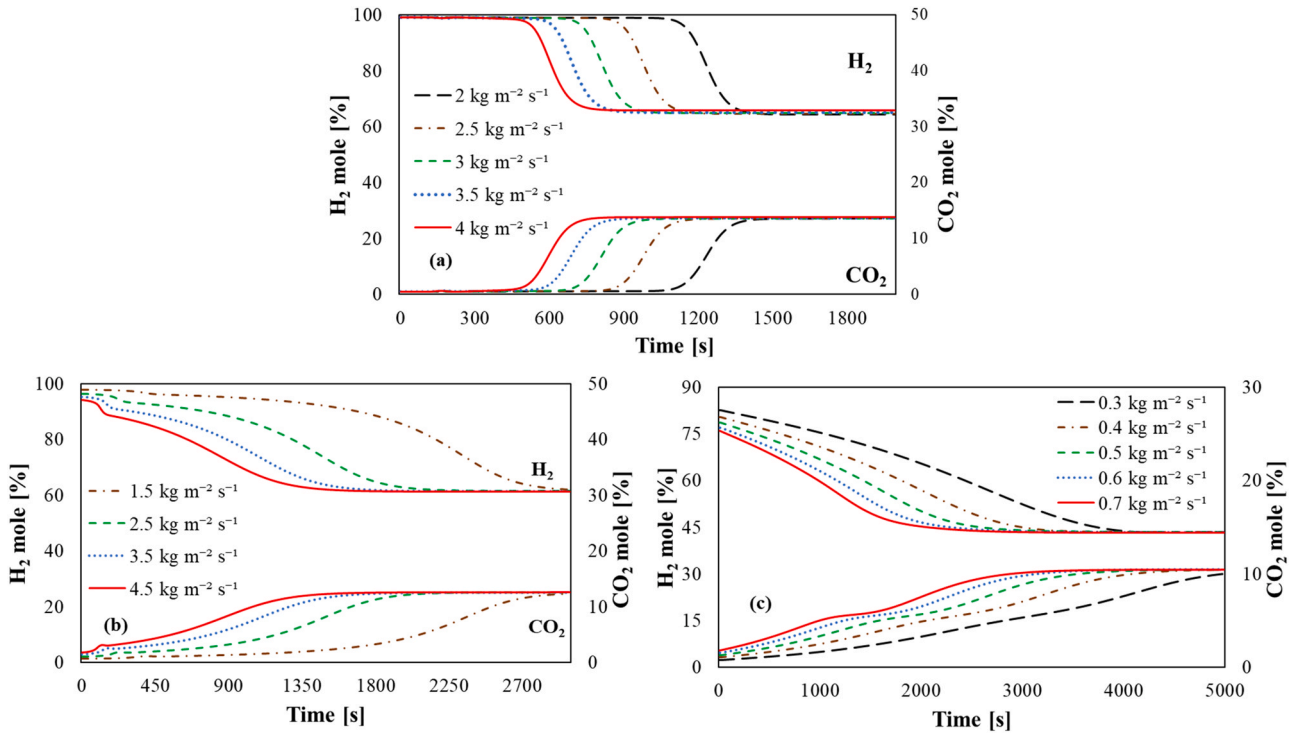

Fig. 10. Effect of G_s on the H_2 and CO_2 molar concentration (dry basis) by using (a) CaO at 900 K, S/C of 3.0 and 3 bar, (b) LZC at 950 K, S/C of 3.0 and 10 bar and (c) HTC at 773 K, S/C of 3.0 and 5 bar.

(0.5 kg m^{-2} s^{-1}) is 7 times smaller than the G_s selected for CaO (3.5 kg m^{-2} s^{-1}).

3.4.4. CH_4 conversion enhancement factor (C_F)

The C_F factor defines the extent of increase in CH_4 conversion when the conventional SMR reactor is loaded with CO_2 adsorbent along with the reforming catalyst, i.e. the comparison of SE-SMR and SMR in terms of CH_4 conversion. It can be used to compare the performance of the various sorbents in terms of fuel conversion. The conversion enhancement CF factor can be quantified by the conversion of methane of methane in the presence of adsorbent $(X_{CH4})_{ad}$ and conversion in the absence of adsorbent $(X_{CH4})_{nad}$, i.e.

$$C_F = \frac{(X_{CH4})_{ad} - (X_{CH4})_{nad}}{(X_{CH4})_{nad}} \times 100 \quad (10)$$

The C_F decreases as the sorbent bed approaches its saturation point and once the adsorbent bed is saturated, CF is zero, which means that the SE-SMR reactor is now acting as a SMR reactor. When the conventional SMR process is transformed into SE-SMR process by the inclusion of sorbent with the catalyst, this results in rise of reformer temperature, which in turn favors the endothermic reforming reactions R1 and R2 and C_F increases. Secondly, the sorbent decreases partial pressure of CO_2 by removing it from the product gas and this results in shifting the chemical equilibrium of reforming reactions R1 and R2 towards more CH_4 conversion. This equilibrium shift results in higher CO partial pressure, thus shifting favourably R3, thereby closing a virtual circle of enhancement of H_2 and CO_2 production and thus C_F factor improves.

Table 3 shows the effect of S/C on C_F for the three sorbents used in this study. CaO gives the value of 40.4% for C_F at S/C of 1. By increasing S/C from 1 to 2, C_F also increases from 40.4% to 71.9%. The sudden increase in C_F is because the steam is introduced from its sub-stoichiometric amount (S/C = 1) of R5 to its stoichiometric amount (S/C =2). Further increase in S/C in the 3 – 4 range decreases the C_F to 67.0–52.9%. Since stoichiometric conditions are not favorable for CH_4 conversion and H_2 purity, a S/C of 3 is selected in this work as the optimum value for all three sorbents. Also, the generation of high S/C requires more heat, so the thermal efficiency of the overall process would decrease.

Table 3
The effect of S/C on C_F for the different CO_2 sorbents.

	CH_4 Conversion Enhancement (C_F)		
S/C	CaO	LZC	HTC
1	40.4	71.6	91.2
2	71.9	118.6	116.1
3	67.0	110.8	113.9
4	52.9	83.0	106.3

LZC and HTC show a similar trend but they give a C_F higher in comparison to CaO because they operate at relatively higher pressures. The C_F of 110.8% and 113.9% are obtained at S/C of 3 using LZC and HTC respectively.

3.5. Comparison of sorbent capacities

The sorption kinetics are another performance parameter considered in the choice of sorbent. The fast kinetics are preferred along with high H_2 purity and CH_4 conversion. Fig. 11 shows the sorption capacity (mol kg^{-1}) of CO_2 with time along the length of the reactor using CaO, LZC and HTC sorbents. Fig. 11 **(a)** displays the dynamic profile of CO_2 sorption over CaO. The sorption capacity curve moves along the length of the reactor at a rate of 0.013 mol_{CO2} kg^{-1} s^{-1}. The sharp curve at the start of the reactor (L = 1 m) shows the rapid sorption of CO_2. The time rate of change of CO_2 sorption over CaO sorbent is almost steady as the CO_2 passes over the reactor bed length. Fig. 11 (b and c) shows the variation of sorption curves along the length of the reactor using LZC and HTC respectively. For LZC and HTC, a sharp peak at the start of the reactor is observed. This is due to the availability of a high partial pressures of CO_2 at the start of the reactor. The maximum rate of sorption at the outlet of the reactor using LZC and HTC are 0.0054 mol_{CO2}

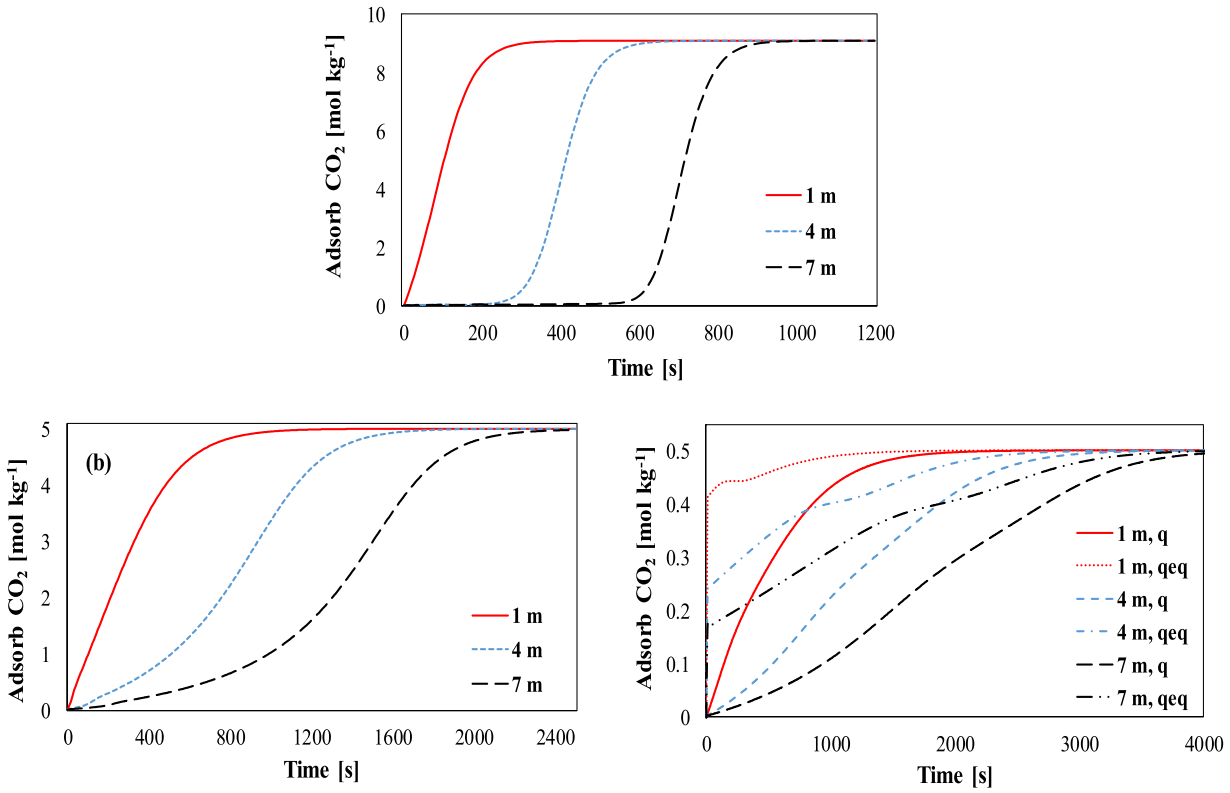

Fig. 11. CO_2 adsorb concentration using (a) CaO at 900 K, S/C of 3.0, 3 bar and G_s of 3.5 kg m^{-2} s^{-1}, (b) LZC at 950 K, S/C of 3.0, 10 bar, and G_s of 2.5 kg m^{-2} s^{-1} and (c) HTC at 773 K, S/C of 3.0, 5 bar and G_s of 0.5 kg m^{-2} s^{-1}.

kg^{-1} s^{-1} and 0.0003 mol_{CO2} kg^{-1} s^{-1} respectively. The low value of CO_2 sorption on HTC as compared to CaO (9 mol_{CO2} kg^{-1} s^{-1}) and LZC (5 mol_{CO2} kg^{-1} s^{-1}) is due to the low sorption capacity (m_{CO2} =0.65 mol_{CO2} kg^{-1} s^{-1}) of HTC. The r_{ads} of HTC is much slower than the r_{ads} of CaO at their optimum conditions.

4. Conclusion

The performance of the SMR process can be significantly improved by using sorbents along with the catalyst during the SMR process. There is a wide portfolio of sorbents available for uptake CO_2 at high temperatures. The choice of these sorbents normally depends upon the CO_2 capture kinetics, sorption capacity, durability and cost. The present mathematical model is capable of predicting the performance of the SE-SMR process in terms of CH_4 conversion, H_2 purity, H_2 yield and CO_2 capture efficiency. A rise in temperature during the pre-breakthrough period is observed using LZC and CaO sorbents. In addition, HTC shows no rise in temperature during the pre-breakthrough period. The highly endothermic nature of the SE-SMR process, using HTC (ΔH^0_{298K} = 191 kJ mol^{-1}_{CH4}), restricts the rise in temperature during the pre-breakthrough period. ΔT_{rise} for CaO and LZC is found to be 17.5 K and 20 K respectively. This shows the highly exothermic nature of these sorbents. A pre-breakthrough period of 690 s, 250 s and 1400 s is observed using CaO LZC and HTC respectively. The optimum pressure and temperature conditions obtained for CaO is 3 bar and 900 K respectively. Temperatures higher than 900 K for CaO causes a decline in H_2 purity and CO_2 capture efficiency whereas, high pressures give low CH_4 conversion. The choice of S/C depends on the overall operational cost of the plant. A S/C higher than 2 would increase the steam production cost. Also, high S/C increases CH_4 conversion and CO_2 capture efficiency. Thus, there is always a tradeoff between CH_4 conversion and overall operational cost of the plant in selecting the S/C.

In terms of the selection of mass flow velocity G_s, it depends on the operational time of the SE-SMR reactor. The optimum S/C and G_s selected using CaO is 3.0 and 3.5 $kgm^{-2}s^{-1}$ respectively. The LZC gives more CH_4 conversion than CaO at 10 bar, 950 K, S/C of 3.0 and 2.5 $kgm^{-2}s^{-1}$. The CO_2 capturing efficiency increases with pressure using LZC, but at very high pressures, the CH_4 conversion decreases quickly. The optimum values for HTC are found to be 773 K, 5 bar, S/C of 3 and 0.5 $kgm^{-2}s^{-1}$. The conversion enhancement factor (C_F) decreases with the increase in S/C from 2 to 4. The C_F for CaO, LZC and HTC are found to be 67%, 110.8% and 113.9% respectively at S/C of 3. Overall, if HTC is used at high temperature (>900 K), it would give high CH_4 conversion, H_2 purity, yield, and CO_2 capture efficiency but its chances of getting decomposed above 773 K limits its use to lower temperatures in comparison to CaO and LZC, which can be used at elevated temperatures. LZC shows good attributes also, however, CaO possesses faster CO_2 capture kinetics than LZC and HTC. In relation to the capture capacity, CaO has a markedly higher capacity than LZC (approx. 2 times) and HTC (approx. 18 times).

CRediT authorship contribution statement

M. Mateen Shahid: Conceptualization, Methodology, Software, Validation, Writing - original draft. **Syed Zaheer Abbas:** Data curation, Software, Validation, Supervision, Writing - review & editing. **Fahad Maqbool:** Visualization, Investigation, Software. **Sergio Ramirez-Solis:** Data curation, Writing - review & editing. **Valerie Dupont:** Supervision, Writing - review & editing. **Tariq Mahmud:** Supervision, Writing - review & editing.

Declaration of Competing Interest

The authors declare that they have no known competing financial interests or personal relationships that could have appeared to influence the work reported in this paper.

Acknowledgement

The following are gratefully acknowledged: to the technical support of Dr. Zainab I. S. G. Adiya in the use of NASA's CEA, the University of Engineering and Technology (UET) Lahore, the EPSRC and the UKCCSRC for Call 2 grant "Novel materials and reforming processing route for the production of ready-separated CO2/N2/H2 from natural gas feedstocks" EP/K000446/1 and Prof. Mojtaba Gadhiri from the University of Leeds, for access to the license for gPROMS modelbuilder. Associated data for this article can be found at https://doi.org/10.5518/1018.

Appendix A. SMR and sorbent kinetic data

A1: The SMR kinetic data along with kinetic rate constants and equilibrium constants;

$$R_1 = \frac{k_1}{p_{H_2}^{2.5}}\left(p_{CH_4}p_{H_2O} - \frac{p_{H_2}^3 p_{CO}}{K_I}\right)\left(\frac{1}{\Omega^2}\right) \quad (A1\text{–}1)$$

$$R_2 = \frac{k_2}{p_{H_2}}p_{CO}p_{H_2O} - \frac{p_{H_2}p_{CO_2}}{K_{III}}\left(\frac{1}{\Omega^2}\right) \quad (A1\text{–}2)$$

$$R_3 = \frac{k_3}{p_{H_2}^{3.5}}\left(p_{CH_4}p_{H_2O}^2 - \frac{p_{H_2}^4 p_{CO_2}}{K_{II}}\right)\left(\frac{1}{\Omega^2}\right) \quad (A1\text{–}3)$$

R_1 is the rate expression for SMR reaction (R1).
R_2 is the rate expression for SMR reaction (R2).
R_3 is the rate expression for WGS reaction (R3).
k_1, k_2 and k_3 are the reaction rate constants for reactions R1, R2 and R3 respectively

$$k_1 = k_{0,1}\exp\left(\frac{-E_1}{RT}\right) = (1.17\times10^{15}) \quad \exp\left(\frac{-240100}{RT}\right) \quad (A1\text{–}4)$$

$$k_2 = k_{0,2}\exp\left(\frac{-E_2}{RT}\right) = (5.43\times10^{5}) \quad \exp\left(\frac{-67130}{RT}\right) \quad (A1\text{–}5)$$

$$k_3 = k_{0,3}\exp\left(\frac{-E_3}{RT}\right) = (2.83\times10^{14}) \quad \exp\left(\frac{-243900}{RT}\right) \quad (A1\text{–}6)$$

$$K_I = \exp\left(\frac{-26830}{T_s} + 30.114\right) \quad (A1\text{–}7)$$

$$K_{II} = \exp\left(\frac{4400}{T_s} - 4.036\right) \quad (A1\text{–}8)$$

$$K_{III} = \quad K_I K_{II} \quad (A1\text{–}9)$$

Kj = thermodynamic equilibrium constant for SMR reactions.

$$\Omega = 1 + K_{CO}p_{CO} + K_{H_2}p_{H_2} + K_{CH_4}p_{CH_4} + K_{H_2O}\frac{p_{H_2O}}{p_{H_2}} \quad (A1\text{–}10)$$

$$K_i = K_{oi}\exp\left(\frac{-\Delta H_i}{R_g T}\right) \quad (A1\text{–}11)$$

Ki = sorption constant for component gaseous 'i'.

A2: Rate equation of CaO sorbent

$$\frac{dq_{CO2}}{dt} = k_{carb}(X_{max} - X)\left(\upsilon_{CO2} - \upsilon_{CO2,eq}\right) \times 1000/56 \quad (A2\text{–}1)$$

Where, q_{CO2}[$mol_{CO2}/kg_{sorbent}$ is the molar concentration of CO_2 adsorb per kg of sorbent. $\upsilon_{CO2,eq}$ is the volumetic fraction of CO_2 at equilibrium conditions.

X_{max} (maximum carbonation conversion) = 0.4.
k_{carb} (rate of carbonation) = 0.35 s^{-1}

$$\upsilon_{CO2,eq} = \left(4.137 \times 10^{7}\right)\exp\left(\frac{-20474}{T}\right) \quad (A2\text{–}2)$$

Maximum carbonation conversion (X_{max}) is given as:

$$X_{max} = 96.34\exp\left(\frac{-12171}{T}\right)4.49\exp\left(\frac{4790.6}{T}\right) \quad (A2\text{–}3)$$

A3: CO_2 sorption kinetics of LZC

$$\frac{dx}{dt} = \quad k_{carb} C_{CO_2}^{n} (1 - x) \tag{A3–1}$$

Where, x = extent of reaction. It is defined as $x = \frac{q_{CO_2}}{q_{CO_2,max}}$.The maximum uptake of CO_2 ($q_{CO_2,max}$) experimentally (reported by Fernandez et al.) is 5.0 $mol_{CO2}Kg^{-1}{}_{sorbent}$.

$k_{carb} = 4.9 \times 10–5\ m^{3n}/mol^{n}s$ (sorption rate constant).

n = 0.93 (order of sorption reaction)

$$r_{ads} = \quad \frac{q_{CO_2,max}}{m_{CO_2}} \quad \frac{dx}{dt} \tag{A3–2}$$

$$k_{carb} = \quad k^{o}_{carb} exp[-\frac{E_{ad}}{R}\left(\frac{1}{T} - \frac{1}{T_o}\right)] \tag{A3–3}$$

E_{ad} (activation energy) $= 8.94 \times 10^4\ Jmol^{-1}$.

$T_o = 673$ K.

A4: HTC sorbent kinetic model

$$r_{ads} = \quad \frac{\partial q_{CO_2}}{\partial t} = \quad k_{carb}(q^{*}_{CO_2} - q_{CO_2}) \tag{A4–1}$$

Where, 'q_{CO_2}' is the equilibrium CO_2 concentration on sorbent, ($mol_{CO2}Kg^{-1}{}_{sorbent}$)

$$k_{carb} = \quad \frac{15}{r_p^2} \quad \frac{\epsilon_p D_p}{\epsilon_p + (1 - \epsilon_p)\rho_p RT(\frac{\partial q^{*}_{CO_2}}{\partial p_{CO_2}})} \tag{A4–2}$$

Where, 'k_{CO_2}' is the sorption constant,

'D_p' is the pore diffusion coefficient, with $1.1 \times 10^{-6}\ m^2s^{-1}$

$$q^{*}_{CO_2} = \quad \frac{m_{CO_2} b_{CO_2} p_{CO_2}}{1 + b_{CO_2} p_{CO_2}} \tag{A4–3}$$

Where, p_{CO_2} = Partial pressure of CO_2 in the gas phase.

m_{CO_2} (maximum sorption capacity of HTC) $= 0.65\ mol_{CO2}Kg^{-1}{}_{sorbent}$.

The temperature dependent Langmuir parameter (b_{CO_2}) is given as;

$$b_{CO_2} = \quad b_{CO_2,ref} exp\left[-\frac{\Delta H_{ads}}{R}\right]\left(\frac{1}{T} - \frac{1}{T_o}\right) \tag{A4–4}$$

Where, ΔH_{ads} (heat of sorption) $= -17 kJmol^{-1}$.

$b_{CO_2,ref} = 23.6 \times 10^{-2}\ kPa^{-1}$.

T_o (reference temperature for b_{CO_2}) = 673 K.

Appendix-B. Empirical correlations

B1 Empirical correlations

$$D_z = 0.73 D_m + \frac{0.5 u_s d_p}{1 + \frac{9.49 D_m}{u_s d_p}} \tag{B1–1}$$

Where, D_z is the axial dispersion coefficient, (m^2s^{-1}).

D_m is the molecular diffusivity, (m^2s^{-1}).

The thermal conductivity($Wm^{-1}K^{-1}$) and mass transfer coefficient ($m^3m^{-2}s^{-1}$) is given as:

$$\frac{\lambda^{f}_z}{\lambda_g} = \frac{\lambda^{o}_z}{\lambda_g} + 0.75 Pr Re_p \tag{B1–2}$$

$$\frac{\lambda^{o}_z}{\lambda_g} = \epsilon_b + \frac{1 - \epsilon_b}{0.139\epsilon_b - 0.0339 + \frac{\left(\frac{2}{3}\right)\lambda_g}{\lambda_s}} \tag{B1–3}$$

$$k_{g,i} = j_{D,i} Re Sc_i^{\frac{1}{3}} \frac{D_i}{d_p} \tag{B1–4}$$

$$\epsilon_b j_{D,i} = 0.765 Re^{-0.82} + 0.365 Sc_i^{-0.398} \tag{B1–5}$$

Dimensionless numbers used in this study is shown by the following relationships:

$$Re = \frac{\rho_f u_s d_p}{\mu}; 0.01 < Re < 1500 \quad \text{(B1–6)}$$

$$Sc_i = \frac{\mu}{\rho_f D_i}; 0.6 < Sc < 7000, 0.25 < \varepsilon_b < 0.96 \quad \text{(B1–7)}$$

$$Pr = \frac{C_{pg}\mu_g}{\lambda_g} \quad \text{(B1–8)}$$

Heat transfer coefficient (h_f) with its dimensionless number (j_H) is given as:

$$h_f = j_H \frac{C_{pg} G_s}{Pr^{\frac{2}{3}}} \quad \text{(B1–9)}$$

$$j_H = 0.91 Re^{-0.51}\psi; 0.01 < Re < 50 \quad \text{(B1–10)}$$

$$j_H = 0.61 Re^{-0.41}\psi; 50 < Re < 1000 \quad \text{(B1–11)}$$

Appendix C. SE-SMR modelling and Rate equations for component 'i'

C-1 SE-SMR reactor modelling equations.

Gas and solid phase material and energy balances;

$$\varepsilon_b\left(\frac{\partial C_i}{\partial t}\right) + \quad \frac{\partial (uC_i)}{\partial z} + k_{g,i}a_v\left(C_i - C_{i,s}\right) = \quad \varepsilon_b D_z \frac{\partial^2 C_i}{\partial z^2} \quad \text{(C1–1)}$$

$$k_{g,i}a_v\left(C_i - C_{i,s}\right) = \upsilon\rho_{cat} r_i - (1-\upsilon) \quad \rho_{ads} r_{ads} \quad \text{(C1–2)}$$

$$\varepsilon_b \rho_g C_{pg}\left(\frac{\partial T}{\partial t}\right) + u\rho_g C_{pg}\frac{\partial (T)}{\partial z} = h_f a_v (T_s - T) + \lambda_z^f \frac{\partial^2 T}{\partial z^2} \quad \text{(C1–3)}$$

$$\rho_{bed} C_{p,bed}\left(\frac{\partial T_s}{\partial t}\right) + h_f a_v (T_s - T) = \upsilon\rho_{cat}\sum - \Delta H_{rxn,j}\eta_j R_j + (1-\upsilon) \quad \rho_{ads}\sum - \Delta H_{ads} r_{ads} \quad \text{(C1–4)}$$

Pressure drop calculations across the reactor bed;

$$\frac{\Delta P g_c}{L} = \frac{150}{d_p^2}\left[\frac{(1-\varepsilon)^2}{\varepsilon^3}\right]\mu u + \left(\frac{1.75}{d_p}\right)\left(\frac{1-\varepsilon}{\varepsilon^3}\right)\rho_g u^2 \quad \text{(C1–5)}$$

Boundary conditions.

At the inlet of reactor i.e. $z = 0$

$$C_i = \quad C_{i,in}; T = T_{in}; T_s = T_{s,in}; P = P_{in}$$

At the outlet of reactor i.e. $z = L$

$$\frac{\partial C_i}{\partial z} = 0; \frac{\partial T}{\partial z} = 0; \frac{\partial T_s}{\partial z} = \quad 0$$

Initial condition

$$C_i = \quad C_{i,0}; T = \quad T_o; T_s = T_{s,o}; q_{CO2} = 0$$

C-2 The rate of formation or consumption of component 'i' is given as:

$$r_i \quad = \sum_{j=1}^{3} \eta_i \varphi_{ij} R_j \quad i = CH_4, CO, CO_2, H_2 \quad \text{and} \quad H_2O \quad \text{(C2–1)}$$

For all component, it is given as;

$$r_{CH_4} = \quad -R_1 - R_2 \quad \text{(C2–2)}$$

$$r_{H_2O} = \quad -R_1 - 2R_2 - R_3 \quad \text{(C2–3)}$$

$$r_{H_2} = \quad 3R_1 + 4R_2 + R_3 \quad \text{(C2–4)}$$

$$r_{CO_2} = \quad R_2 + R_3 \quad \text{(C2–5)}$$

$$r_{CO} = \quad R_1 - R_3 \quad \text{(C2–6)}$$

where, φ_{ij} is the stoichiometric coefficient. The value of φ_{ij} is negative for reactants and positive for products.

References

[1] J.P. Jakobsen, E. Halmøy, Reactor modeling of sorption enhanced steam methane reforming, Energy Procedia 1 (1) (2009) 725–732.
[2] D.P. Harrison, Sorption-enhanced hydrogen production: a review, Ind. Eng. Chem. Res. 47 (17) (2008) 6486–6501.
[3] J.R. Fernandez, J.C. Abanades, R. Murillo, Modeling of sorption enhanced steam methane reforming in an adiabatic fixed bed reactor, Chem. Eng. Sci. 84 (2012) 1–11.
[4] L. Barelli, G. BIDINI, F. GALLORINI, S. SERVILI, Hydrogen production through sorption-enhanced steam methane reforming and membrane technology: a review, Energy 33 (4) (2008) 554–570.
[5] J.M. Silva, R. Trujillano, V. Rives, M.A. Soria, L.M. Madeira, High temperature CO_2 sorption over modified hydrotalcites, Chem. Eng. J. 325 (2017) 25–34.
[6] A.L. García-Lario, G.S. Grasa, R. Murillo, Performance of a combined CaO-based sorbent and catalyst on H2 production, via sorption enhanced methane steam reforming, Chem. Eng. J. 264 (2015) 697–705.
[7] J.R. Hufton, S. Mayorga, S. Sircar, Sorption-enhanced reaction process for hydrogen production, AIChE J. 45 (2) (1999) 248–256.
[8] B. Balasubramanian, A. Lopez Ortiz, S. Kaytakoglu, D.P. Harrison, Hydrogen from methane in a single-step process, Chem. Eng. Sci. 54 (15–16) (1999) 3543–3552.
[9] K.B. Yi, D.P. Harrison, Low-pressure sorption-enhanced hydrogen production, Ind. Eng. Chem. Res. 44 (6) (2005) 1665–1669.
[10] B. Arstad, J. Prostak, R. Blom, Continuous hydrogen production by sorption enhanced steam methane reforming (SE-SMR) in a circulating fluidized bed reactor: sorbent to catalyst ratio dependencies, Chem. Eng. J. 189 (2012) 413–421.
[11] K. Johnsen, J.R. Grace, S.S.E.H. Elnashaie, L. Kolbeinsen, D. Eriksen, Modeling of sorption-enhanced steam reforming in a dual fluidized bubbling bed reactor, Ind. Eng. Chem. Res. 45 (12) (2006) 4133–4144.
[12] Y. Huang, S. Rebennack, Q.P. Zheng, Techno-economic analysis and optimization models for carbon capture and storage: a survey, Energy Syst. 4 (4) (2013) 315–353.
[13] S.Z. Abbas, V. Dupont, T. Mahmud, Modelling of H2 production in a packed bed reactor via sorption enhanced steam methane reforming process, Int. J. Hydrog. Energy 42 (30) (2017) 18910–18921.
[14] B.K. Dutta, Principles of mass transfer and separation processes, Can. J. Chem. Eng. 87 (5) (2009) 818–819.
[15] E. Ochoa-Fernández, G. Haugen, T. Zhao, M. Rønning, I. Aartun, B. Børresen, E. Rytter, M. Rønnekleiv, D. Chen, Process design simulation of H 2 production by sorption enhanced steam methane reforming: evaluation of potential CO 2 acceptors, Green. Chem. 9 (6) (2007) 654–662.
[16] S. Kumar, S.K. Saxena, A comparative study of CO 2 sorption properties for different oxides, Mater. Renew. Sustain. Energy 3 (3) (2014) 30.
[17] M.S. Yancheshmeh, H.R. Radfarnia, M.C. Iliuta, High temperature CO_2 sorbents and their application for hydrogen production by sorption enhanced steam reforming process, Chem. Eng. J. 283 (2016) 420–444.
[18] Roger, W., Hydrogen production. 1933, Google Patents.
[19] D.K. Lee, I.H. Baek, W.L. Yoon, Modeling and simulation for the methane steam reforming enhanced by in situ CO_2 removal utilizing the CaO carbonation for H2 production, Chem. Eng. Sci. 59 (4) (2004) 931–942.
[20] C. Han, D.P. Harrison, Simultaneous shift reaction and carbon dioxide separation for the direct production of hydrogen, Chem. Eng. Sci. 49 (24) (1994) 5875–5883.
[21] M. Xie, Z. Zhou, Y. Qi, Z. Cheng, W. Yuan, Sorption-enhanced steam methane reforming by in situ CO_2 capture on a CaO–Ca9Al6O18 sorbent, Chem. Eng. J. 207 (2012) 142–150.
[22] H.K. Rusten, E. Ochoa-Fernández, D. Chen, H.A. Jakobsen, Numerical investigation of sorption enhanced steam methane reforming using Li2ZrO3 as CO_2-acceptor, Ind. Eng. Chem. Res. 46 (13) (2007) 4435–4443.
[23] M.H. Halabi, M.H.J.M. de Croon, J. van der Schaaf, P.D. Cobden, J.C. Schouten, Reactor modeling of sorption-enhanced autothermal reforming of methane. Part I: performance study of hydrotalcite and lithium zirconate-based processes, Chem. Eng. J. 168 (2) (2011) 872–882.
[24] Y. Ding, E. Alpay, Equilibria and kinetics of CO_2 adsorption on hydrotalcite adsorbent, Chem. Eng. Sci. 55 (17) (2000) 3461–3474.
[25] E. Ochoa-Fernández, H.K. Rusten, H.A. Jakobsen, M. Rønning, A. Holmen, D. Chen, Sorption enhanced hydrogen production by steam methane reforming using Li2ZrO3 as sorbent: sorption kinetics and reactor simulation, Catal. Today 106 (1–4) (2005) 41–46.
[26] J. Xu, G.F. Froment, Methane steam reforming, methanation and water-gas shift: I. Intrinsic kinetics, AIChE J. 35 (1) (1989) 88–96.
[27] V. Nikulshina, M.E. Galvez, A. Steinfeld, Kinetic analysis of the carbonation reactions for the capture of CO_2 from air via the Ca (OH) 2–CaCO3–CaO solar thermochemical cycle, Chem. Eng. J. 129 (1–3) (2007) 75–83.
[28] N. Rodríguez, M. Alonso, J.C. Abanades, Experimental investigation of a circulating fluidized-bed reactor to capture CO_2 with CaO, AIChE J. 57 (5) (2011) 1356–1366.
[29] R. Xiong, J. Ida, Y.S. Lin, Kinetics of carbon dioxide sorption on potassium-doped lithium zirconate, Chem. Eng. Sci. 58 (19) (2003) 4377–4385.
[30] K.B. Yi, D.Ø. Eriksen, Low temperature liquid state synthesis of lithium zirconate and its characteristics as a CO_2 sorbent, Sep. Sci. Technol. 41 (2) (2006) 283–296.
[31] E. Ochoa-Fernández, T. Zhao, M. Rønning, D. Chen, Effects of steam addition on the properties of high temperature ceramic CO 2 acceptors, J. Environ. Eng. 135 (6) (2009) 397–403.
[32] M.H. Halabi, M.H.J.M. de Croon, J. van der Schaaf, P.D. Cobden, J.C. Schouten, A novel catalyst–sorbent system for an efficient H2 production with in-situ CO_2 capture, Int. J. Hydrog. Energy 37 (6) (2012) 4987–4996.
[33] E.L. Lugo, B.A. Wilhite, A theoretical comparison of multifunctional catalyst for sorption-enhanced reforming process, Chem. Eng. Sci. 150 (2016) 1–15.
[34] W. Dietrich, P. LAWRENCE, M. GRUNEWALD, D. AGAR, Theoretical studies on multifunctional catalysts with integrated adsorption sites, Chem. Eng. J. 107 (1–3) (2005) 103–111.
[35] F. Maqbool, S.Z. Abbas, S. Ramirez-Solis, V. Dupont, T. Mahmud, Modelling of one-dimensional heterogeneous catalytic steam methane reforming over various catalysts in an adiabatic packed bed reactor, Int. J. Hydrog. Energy 46 (7) (2021) 5112–5130.
[36] B. Dou, V. Dupont, P.T. Williams, H. Chen, Y. Ding, Thermogravimetric kinetics of crude glycerol, Bioresour. Technol. 100 (9) (2009) 2613–2620.
[37] H.H. Faheem, H.U. Tanveer, S.Z. Abbas, F. Maqbool, Comparative study of conventional steam-methane-reforming (SMR) and auto-thermal-reforming (ATR) with their hybrid sorption enhanced (SE-SMR & SE-ATR) and environmentally benign process models for the hydrogen production, Fuel 297 (2021), 120769.
[38] R.J. Kee, F.M. Rupley, J.A. Miller, Chemkin-II: A Fortran chemical kinetics package for the analysis of gas-phase chemical kinetics, Sandia National Lab.(SNL-CA), Livermore, CA (United States), 1989.
[39] S. Gordon, B.J. McBride, Computer program for calculation of complex chemical equilibrium compositions and applications, Part 1: Anal. (1994).
[40] B.J. McBride, Computer Program for Calculation of Complex Chemical Equilibrium Compositions and Applications, NASA Lewis Research Center, 1996.
[41] D. Chattaraj, Structural, electronic, elastic and thermodynamic properties of Li2ZrO3: A comprehensive study using DFT formalism, J. Nucl. Mater. 496 (2017) 286–292.
[42] E.H.P. Cordfunke, R.R. Van Der Laan, G.P. Wyers, J.C. Van Miltenburg, The heat capacities and derived thermophysical properties of Li2ZrO3 and Li8ZrO6 at temperatures from 0 to 1000 K, J. Chem. Thermodyn. 24 (12) (1992) 1251–1256.
[43] A. Antzara, E. Heracleous, D.B. Bukur, A.A. Lemonidou, Thermodynamic analysis of hydrogen production via chemical looping steam methane reforming coupled with in situ CO_2 capture, Int. J. Greenh. Gas. Control 32 (2015) 115–128.
[44] Pans Castillo, M.Á., et al., Optimization of H2 production with CO2 capture by steam reforming of methane integrated with a chemical-looping combustion system. 2013.
[45] H.T.J. Reijers, S.E.A. Valster-Schiermeier, P.D. Cobden, R.W. van den Brink, Hydrotalcite as CO_2 sorbent for sorption-enhanced steam reforming of methane, Ind. Eng. Chem. Res. 45 (8) (2006) 2522–2530.
[46] J. Pérez-Ramírez, S. Abelló, Thermal decomposition of hydrotalcite-like compounds studied by a novel tapered element oscillating microbalance (TEOM): comparison with TGA and DTA, Thermochim. Acta 444 (1) (2006) 75–82.
[47] N.D. Hutson, S.A. Speakman, E.A. Payzant, Structural effects on the high temperature adsorption of CO_2 on a synthetic hydrotalcite, Chem. Mater. 16 (21) (2004) 4135–4143.